Cite this article
Bradley AC, Jaksa MB and Kuo YL (2019)
Examining the kinematics and energy of the four-sided impact roller.
Proceedings of the Institution of Civil Engineers – Ground Improvement **172(4)**: 297–304,
https://doi.org/10.1680/jgrim.18.00124

Research Article
Paper 1800124
Received 07/12/2018;
Accepted 28/02/2019;
Published online 25/06/2019

Keywords: energy/field testing & monitoring/granular materials

Ground Improvement

ice Publishing

Examining the kinematics and energy of the four-sided impact roller

1 **Andrew C. Bradley**
School of Civil, Environmental and Mining Engineering, University of Adelaide, SA, Australia (corresponding author: andrew.bradley@adelaide.edu.au)

2 **Mark B. Jaksa**
School of Civil, Environmental and Mining Engineering, University of Adelaide, SA, Australia

3 **Yien-Lik Kuo**
School of Civil, Environmental and Mining Engineering, University of Adelaide, SA, Australia



The soil-improvement method rolling dynamic compaction (RDC) utilises the mechanical energy imparted by an 'impact roller' module as it is towed. The motion exhibited by this module and the energy delivered into the soil has not yet been addressed in the literature. The kinematics of RDC, with particular reference to the four-sided 8 t impact roller, was investigated in this study. The motion of the module was examined in the field using high-speed photography. Vector velocities of the rolling module were obtained for the impact roller passing over a controlled test bed at a typical operating speed of 10 km/h. It was observed that the module delivered an average of 23 ± 4 kJ per blow to the soil.

Notation

E_{Roller}	total energy of roller
h_{Roller}	height of roller's centroid above ground surface
I_{Roller}	mass moment of inertia of roller
m_{Roller}	mass of roller
r	centroid of module
V_x	horizontal velocity
V_y	vertical velocity
θ	module orientation
ω_x	angular velocity

1. Introduction

Rolling dynamic compaction (RDC) is the generic term adopted to describe the ground-improvement process involving compaction by means of a non-cylindrical rolling module incorporating three, four or five sides. The module rotates about its corners as it is towed and falls to the ground, compacting it dynamically. Recently, this technique has become increasingly adopted in the applications of the densification of subgrade soils, proof rolling and the construction of mine haul roads. The effectiveness of RDC in relation to these applications and how it may be estimated is largely ill-defined, resulting in the need to undertake sometimes costly field trials.

Within the literature it is well documented that the field compactive effort, or energy, applied to the ground is directly related to the geotechnical characteristics of the underlying soil profile. This is regularly observed when comparing the results of standard (ASTM, 2012a; SA, 2003a) and modified Proctor compaction tests (ASTM, 2012b; SA, 2003b). Performed in the laboratory, these tests quantify the dependence of the representative compactive energy and moisture content with respect to the resulting density, which is particular to the soil tested. A single field study conducted by Scott *et al.* (2012) found that the densification of underlying soil subject to RDC, using a Broons BH-1300 8 t four-sided impact roller (Figure 1), was reasonably well represented by means of the modified Proctor test. However, the energy imparted by the module with each impact of the four-sided RDC roller, has yet to be determined with confidence.

To date, only the total potential energy of the BH-1300 impact roller has been investigated in a study by Clifford and Bowes (1995), who suggested that the kinetic energy of the module at impact lies between 50 and 70 kJ. However, as demonstrated later in this paper, this is not the same as the energy delivered to the soil for the purposes of densification. The derivations of Clifford and Bowes were based on highly idealised assumptions, using a cuboid pivoting about a pinned corner, which was calculated at the time of impact along a planar surface and did not explicitly state the magnitude of the energy imparted or delivered to the soil during impact. Avalle *et al.* (2009), on the contrary, suggested that the rolling action of RDC would impart energy over the curved face of the roller and distribute the load non-uniformly. Although the shape is

Figure 1. Broons BH 1300 8 t four-sided impact roller

similar to a square, the curved features of the roller are likely to contribute to this distribution over the full range of the module's motion. Furthermore, the undulating ground surface profile characteristic of RDC, along with the module's double-linkage spring mechanism, among other factors, were not explicitly considered in the analysis performed by Clifford and Bowes (1995). Instead, they somewhat subjectively increased the fall speed by 20% to account for these factors. Despite the idealisations of their study, it nevertheless provides a useful benchmark estimate for the total kinetic energy of the roller against field-measured estimates.

In addition to the lack of understanding of the compactive energy imparted by RDC, the general kinematics of these modules are also largely unclear. In efforts to quantify the effectiveness of RDC, Kuo *et al.* (2013); Bradley *et al.* (2012); Bastaee and Parvizi (2012) and Kim (2010) adopted the finite-element numerical modelling approach. These studies, however, have the common limitation of adopting an assumed constant motion of the module based on approximations. By assuming the roller's motion, the magnitude of the compactive energy imparted to the modelled underlying soil within these numerical studies is not necessarily representative of the module's true behaviour. Understandably, these assumptions were made largely due to the absence of information regarding the kinematics of, and the energy imparted by, the module.

First, this paper aims to describe the general motion of the Broons BH-1300 8 t four-sided roller by means of high-speed photography. Second, the paper seeks to estimate the kinematic profile of the roller to describe its range of motion and thus provide an estimate of the average energy delivered to the ground by the module under typical operating conditions.

2. Field trial

A field trial was undertaken at Monarto Quarry, approximately 60 km south of Adelaide, Australia, to measure directly the influence of the Broons BH-1300 8 t four-sided impact roller on the underlying ground profile. In brief, a 12 m × 7·5 m test pit was excavated to 1·5 m depth and backfilled with a local pale-brown sandy gravel fill material. Underlying the test pit, a natural red–orange gravelly sand of medium-dense consistency was exposed. The particle size distributions for each of these soils are presented in Figure 2.

After excavating the test pit, it was subsequently filled in loose, 0·5 m lifts and preloaded using a 23 t front-end loader to level the ground and improve trafficability prior to RDC. Nuclear density meter testing was adopted to measure the consistency of each lift during filling. The moisture content of the soil was maintained at approximately below optimum moisture content using the methodology suggested by Scott *et al.* (2012).

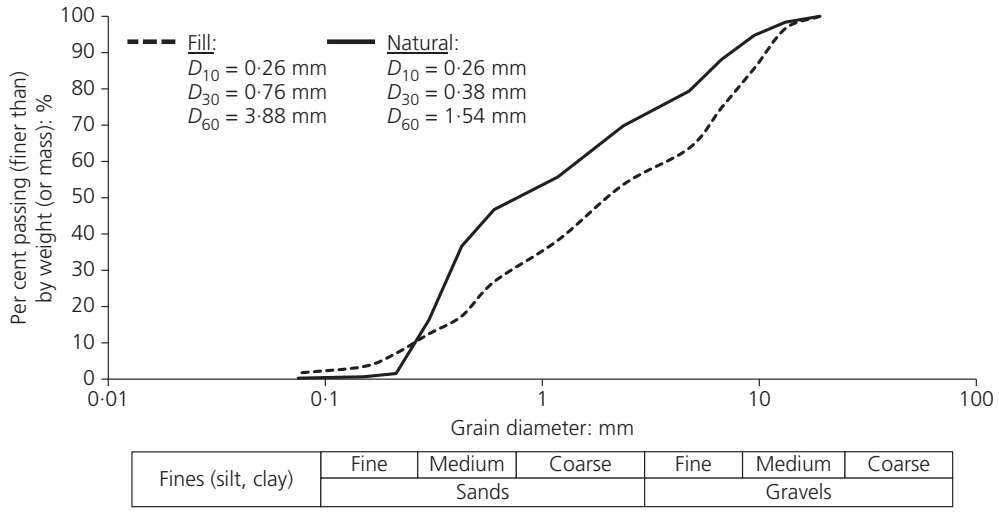

Figure 2. Particle size distributions

The test pit was sub-divided into three 2·5 m wide lanes, identified as lanes A, B and C, and each subjected to 5, 10 and 30 passes, respectively, as indicated in Figure 3. For the purposes of this study, only lane C is considered.

A high-speed digital video camera, capturing 1000 frames/s (fps) at a resolution of 1280×1024 pixels, was located 20 m from lane C and oriented orthogonally to the direction of travel, as shown in Figure 3. By filming at a distance, the camera had a field of view capable of recording up to one complete revolution of the module and was subjected to minimised ground vibrations that would otherwise compromise the quality of the captured images.

The motion of the BH-1300 8 t four-sided impact roller was recorded under typical operating conditions for the compaction of a controlled fill material, which involves being drawn behind a tractor performing 30 passes and directed to travel at a speed of approximately 10 km/h. To improve the accuracy of the tractor's speed, a laser-based measuring tool was installed on the undercarriage of the tractor to display, in real-time for the operator, the tractor's velocity. Furthermore, to ensure the desired tractor speed was maintained across the test pit, the tractor had an approximate 30 m lead up so that the velocity could be achieved and maintained prior to reaching the test pit.

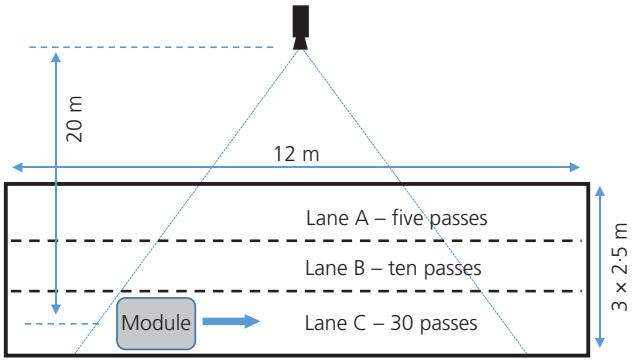

Figure 3. Plan view of field test layout

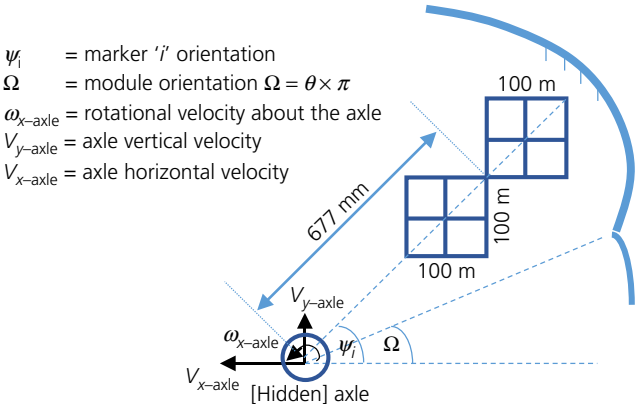

Figure 4. Layout and dimensions of grid markers shown in one quadrant of the four-sided module

To measure the motion of the module, markers of specified dimensions and positions were engraved into the four corners of the module's open face, as shown in Figure 4 and which can also be seen in Figure 1. They were located such that at least one of the four marker pairs was visible to the camera and unobstructed by the chassis frame during operation, enabling the position of the module's axle and rotational velocity to be estimated throughout each pass.

3. Analysis of module motion

To trace the position of the markers within each captured frame, the video recordings of the module were embedded into an open-source image-tracking software package (Brown, 2016) (Figure 5). This software facilitated calculation of the vector velocities. To minimise noise within the data set due to ground vibrations and its effect on the camera, as well as errors associated with video resolution, the frame rate of the recordings was reduced to 50 and 250 fps. Additionally, by estimating the movement of the background, the vibration of the camera could be accounted for and corrected within the data, an example of which is shown in Figure 6. As observed, 50 fps provided a satisfactory resolution of the module's overall motion while sufficiently mitigating noise in the data.

The module's axle position and vertical (V_y), horizontal (V_x) and angular (ω_x) velocities were calculated with respect to the markers. To smooth the data and align overlapping rotations, the axle position was then subject to a zero-lag, fourth-order Butterworth low-pass filter, with a cut-off frequency set at 247·5 Hz. Similarly, the angular velocities were processed using a cut-off frequency of 87·5 Hz. Although not always, the use of the filter generated abnormalities at the start and end of the data sets. To account for possible anomalies, the data sets were truncated to 0·1–1·5 s for each pass. Due to time constraints in the field, analysis was undertaken on passes 1–10, and subsequently every fifth pass. Given V_y, V_x and ω_x time histories, the kinematics of the module for each pass were estimated. A typical result (i.e. for pass 1) is presented in Figure 7.

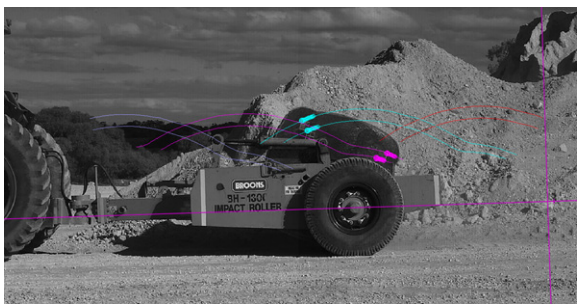

Figure 5. Example of markers being traced as the impact roller passes

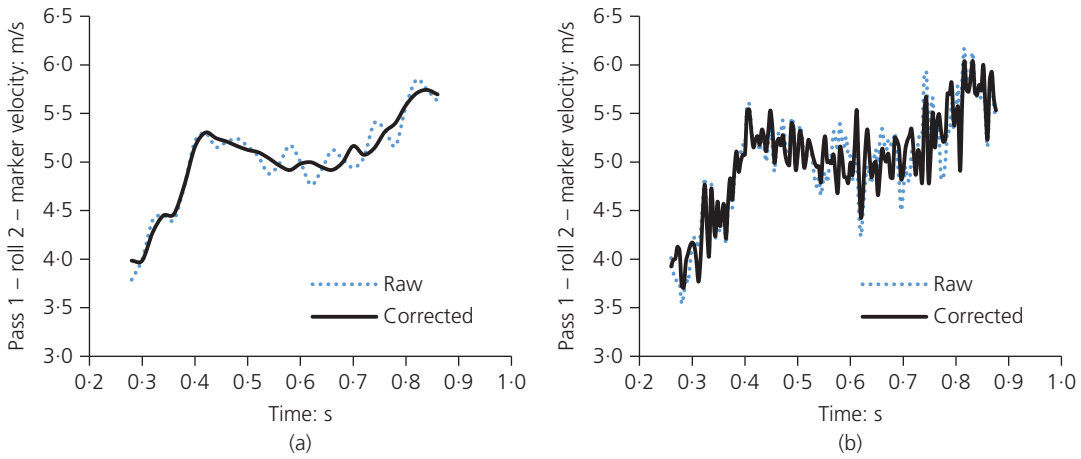

Figure 6. Typical marker velocities measured at (a) 50 fps and (b) 250 fps

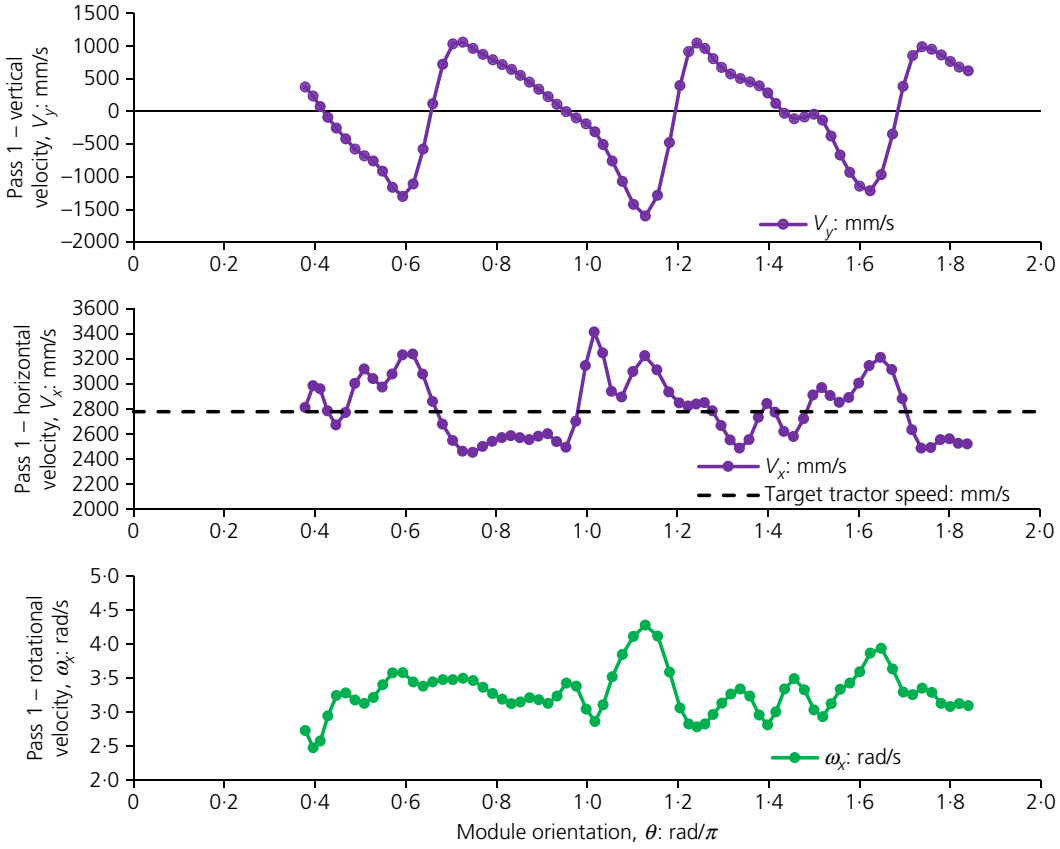

Figure 7. Estimated kinematics measured at or about the roller axle – pass 1

Assuming the energy of the system solely involves the kinematics of a rigid module (i.e. there are no thermal or noise losses and no deformations of the module itself), the total energy of the roller, E_{Roller}, is calculated from Equation 1 and is presented in Figure 8 for pass 1

1. $$E_{\text{Roller}} = E_{\text{Kinetic}} + E_{\text{Potential}}$$

2. $$E_{\text{Kinetic}} = 1/2 m_{\text{Roller}}\left(V_x^2 + V_y^2\right) + 1/2 I_{\text{Roller}}\omega_x^2$$

3. $$E_{\text{Potential}} = m_{\text{Roller}} g h_{\text{Roller}}$$

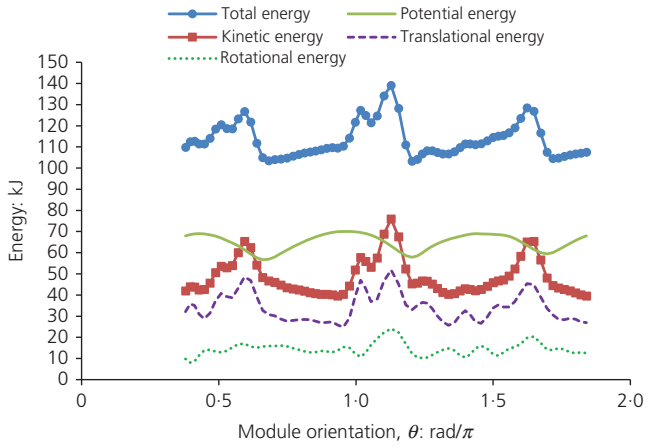

Figure 8. Estimated energy profile – pass 1

where m_{Roller} is the mass of the roller, I_{Roller} is the mass moment of inertia of the roller, $\boldsymbol{g}$ is acceleration due to gravity and h_{Roller} is the height of the roller's centroid above the ground surface. Note that the kinetic energy is a combination of translational and rotational energies, as shown in Equation 2 and Figure 8.

The mass moment of inertia of the roller, I_{Roller}, is calculated from Equation 4 and, by transforming the design specifications of the BH-1300 8 t four-sided module to their radial lengths with respect to the module's centroid, r, and mass, m, I_{Roller} was found to be equal to $2{\cdot}631 \times 10^9$ kg mm^2.

$$4. \quad I_{\text{Roller}} = \int r^2 \, \mathrm{d}m$$

To estimate h_{Roller}, the initial height of the module's centroid was obtained from the design geometry of the module as though in contact with an undeformed soil surface at a null rotational angle, $\Omega = 0$. Thereafter, h_{Roller} was evaluated with respect to the estimated V_y for each pass.

Given the energy profiles for each pass, it is possible to explore whether or not a relationship exists between the derived energies, the number of passes and the tractor speed; in particular, the peak kinetic energy of the roller and the peak total energy lost with each impact. To do so, it is assumed that the majority, if not all, of the roller's energy is delivered directly to the ground. This is in contrast with the system not being perfectly isolated and the energy of the roller being lost due to several factors. These include, but are not limited to thermal, noise, compressional and internal damping losses from the module itself, and that lost or gained by the interactions with the chassis frame through the double-linkage spring mechanism within the range of impact. These are expected to be minor and the magnitude of these losses is not explored in this study. The results are presented in Figure 9, where the tractor speed is averaged over each pass.

A well-established characteristic of RDC is that the ground surface becomes more undulating with each successive module pass. As a result, one would expect the module motion to be influenced by the evolving shape and condition of the ground surface. In this case, however, the results in Figure 9 suggest otherwise. This is likely the result of a combination of factors, including, but not limited to, the initial ground condition, tractor speed and roller weight.

It can be observed from Figure 9(a) that the desired 10 km/h tractor speed was achieved within an acceptable tolerance. Given this rather small variation in tractor speed, there is no compelling evidence to suggest that the kinetic energy or the energy delivered to the ground were affected by the tractor speed. However, in order to derive a more generic conclusion of this nature, further field trials are needed that involve a

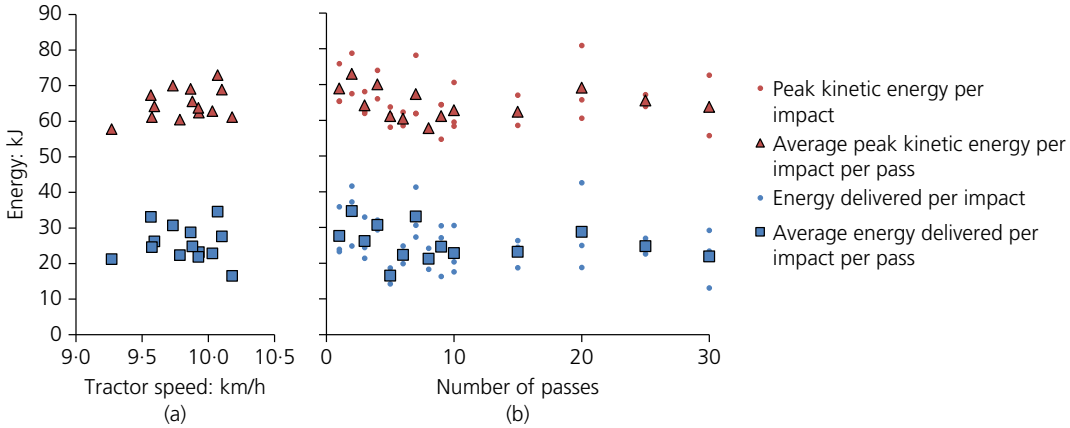

Figure 9. Estimated peak kinetic energy and that delivered for each impact with respect to (a) estimated tractor speed and (b) number of passes

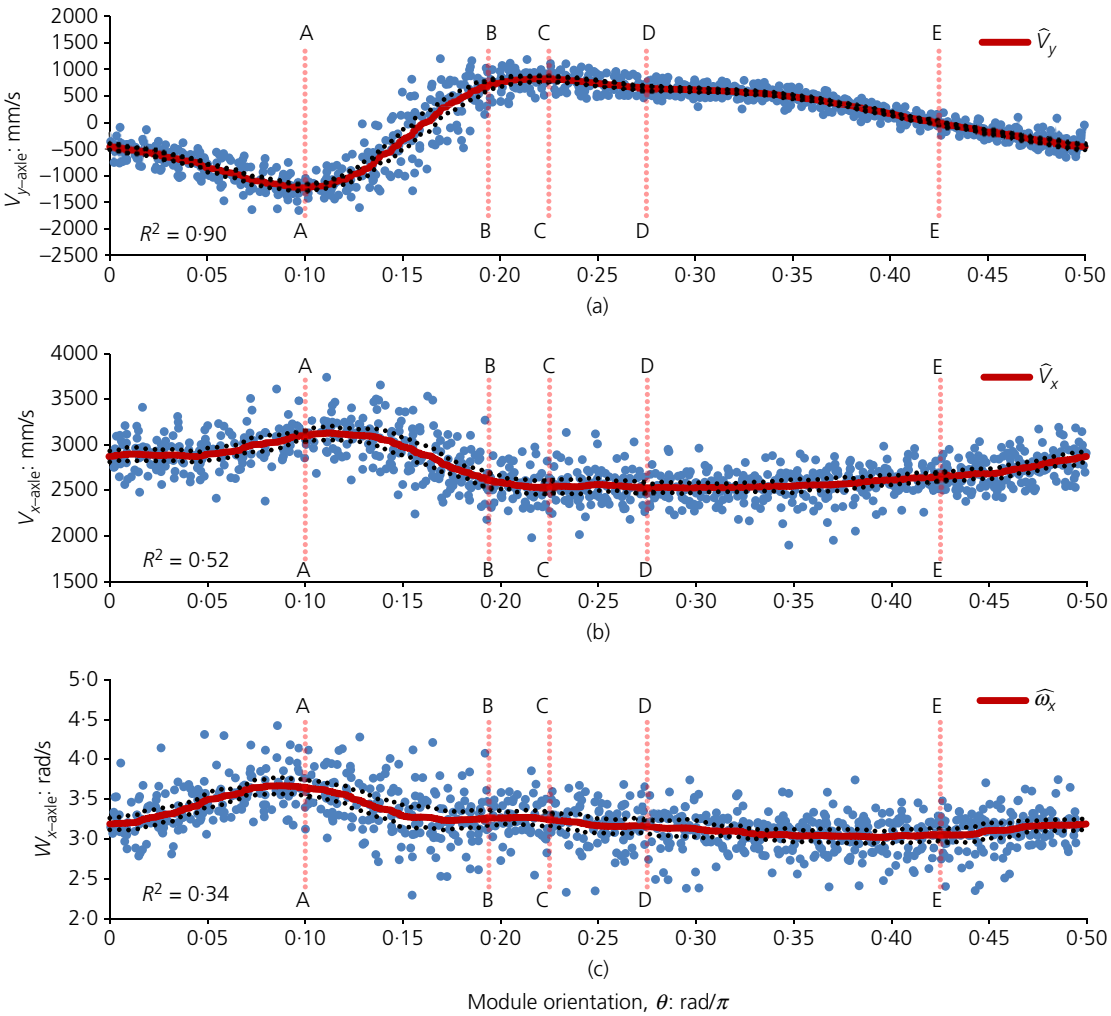

Figure 10. Low-pass filtered results with local 95% confidence intervals: (a) vertical velocity – period of 0·5; (b) horizontal velocity – period of 0·5; (c) angular velocity – period of 0·5

greater range of tractor speeds. Such trials were beyond the scope of this study.

3.1 Estimation of a representative kinematic profile

In response to there being no clear dependence on the number of passes, the towing speed and the motion of the module, a typical motion, representative over all 30 passes, was investigated. This was undertaken to simplify the results into a single representative trend by again applying a zero-lag, fourth-order Butterworth low-pass filter to the data.

The roller clearly exhibited a sinusoidal-like cyclic behaviour as it lifted and fell while being towed. With this in mind, modular periods of one-quarter ($\pi/2$ rad) and one-half (π rad) of one revolution of the module were considered to examine the repeatable nature of the module's motion. The time histories for V_y, V_x and ω_x were superimposed over each period of the module's rotation. The data set was then replicated into a series to capture the repeatable nature of the module's motion. The filter was independently applied to V_y, V_x and ω_x to produce the filtered time histories of $\widehat{V_y}$, $\widehat{V_x}$ and $\widehat{\omega_x}$, which express the typical motion; a one-quarter revolution period is presented in Figure 10.

Appearing as though superimposed, there was no significant difference between the one-quarter and one-half revolutions. It is thus reasonable to conclude that the representative typical motion of the module may be taken as being identical to each one-quarter revolution.

To evaluate the amount of energy that is imparted to the ground conceptually, it is necessary to assess the time histories of $\widehat{V_y}$, $\widehat{V_x}$ and $\widehat{\omega_x}$ in conjunction with the phases of the roller's motion. By scrutinising the video recordings and the $\widehat{V_y}$, $\widehat{V_x}$ and $\widehat{\omega_x}$ time histories, the motion of the four-sided roller was

subdivided into five phases of motion for every one-quarter of a single revolution. These are defined as the impact (A–A to B–B), corner-suspended (B–B to C–C), sliding (C–C to D–D), tripping (D–D to E–E) and falling (E–E to A–A) phases, as indicated in Figure 11. While the transitions between each of the phases appear to vary within a given range of orientation (which reflects the range of motion possible), approximations for these phases were assigned. Hence, the gain or loss of the module's energy may be quantified and better understood with respect to its phase of motion. By assuming the impact phase A–A to be wholly representative of the period when the energy of the roller is transferred to the ground, the magnitude of energy imparted for compaction purposes may be quantified.

Additionally, by estimating the standard deviation locally, with respect to each data point using a moving window operation, the variability of the field measurements can be evaluated. The range of the moving window was investigated so as to obtain optimal results. This was achieved by varying the width of the moving window in terms of the number of adjacent data points included in the standard deviation calculations for the vertical, horizontal and rotational velocities. As shown in Figure 12, it is clear that the standard deviation, and its smoothness, was dependent on the moving window width. As can be seen, a moving window width of 31 data points provided a good compromise between overly smoothed (i.e. 241 wide) and highly variable (i.e. 15 wide) results. Hence, it can be concluded, with 95% confidence, that each of the roller's impacts transferred on average 23 ± 4 kJ to the ground, as presented in Figure 13.

As shown in Figure 13, the kinetic energy at the inception of impact (A–A) ranged from 50–80 kJ, with an average value of 62 ± 3 kJ, with 95% confidence. These observations align well with the 50–70 kJ range suggested by Clifford and Bowes (1995), as discussed earlier, which includes some degree of subjectivity.

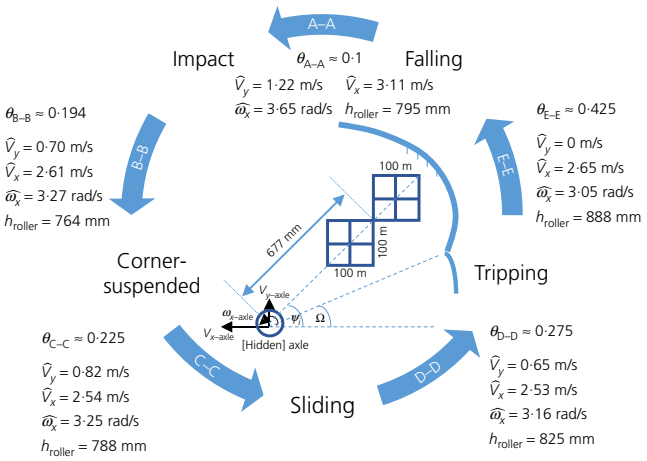

Figure 11. Suggested phases of motion for the four-sided impact roller

4. Conclusions

This study sought to describe the general motion of an 8 t four-sided impact roller (Broons BH-1300) by means of high-speed photography and to quantify the energy delivered to the ground. The motion of the roller was subdivided into five distinct phases: impact, corner-suspended, sliding, tripping and falling. By examining the kinematics of the module, it is concluded that the energy delivered to the ground by the four-sided module, under typical operating conditions, is 23 ± 4 kJ per impact with a 95% degree of confidence. A total of 30 passes was examined and there was no evidence to suggest that the delivered energy was affected by the number of passes. As a consequence of needing to constrain the operational speed of the tractor in the field, it was not possible to examine the extent to which the delivered energy was affected by the towing velocity. Finally, examination of the kinematics of the impact

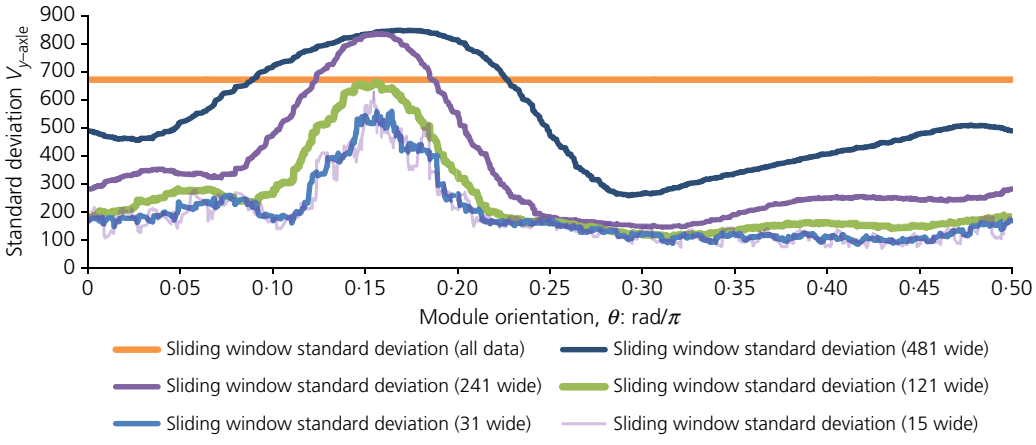

Figure 12. Sliding window standard deviation for vertical velocity – period of 0·5. A full-colour version of this figure can be found on the ICE Virtual Library (www.icevirtuallibrary.com)

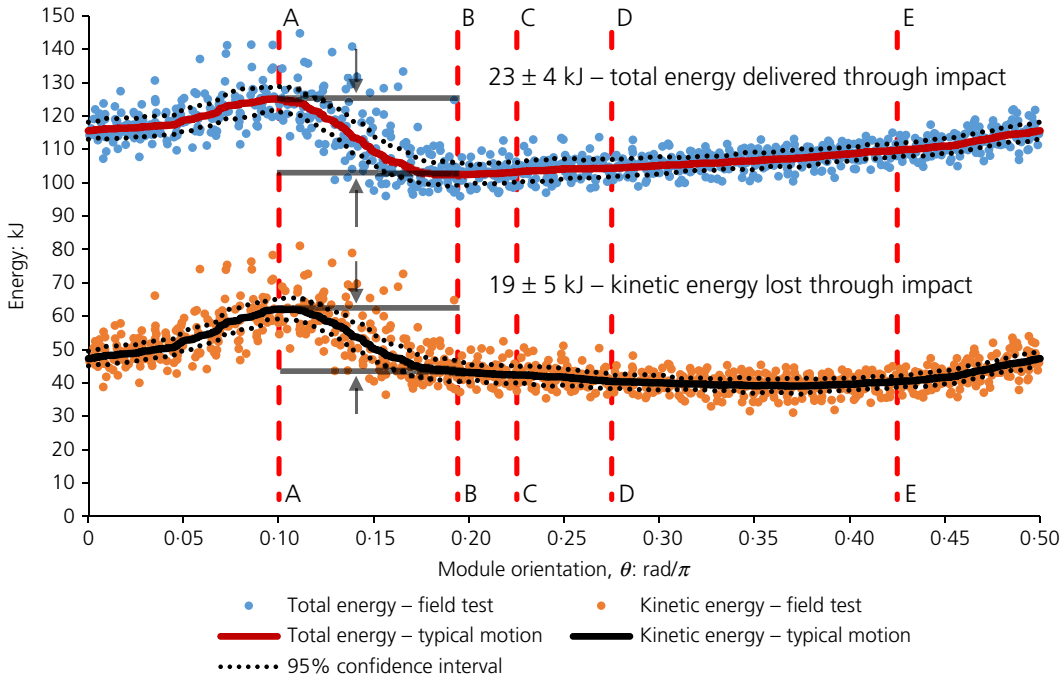

Figure 13. Estimates of total and kinetic energy of the impact roller with 95% confidence intervals – period of 0·5

roller revealed remarkable reproducibility of the module's motion with successive rotations.

Acknowledgements

The authors are grateful to Mr Stuart Bowes and the staff at Broons for their assistance in the provision of the impact roller used in the field study. The authors also appreciate the assistance of Drs Mellissa Humphries, Will Robertson and John Codrington at the University of Adelaide.

REFERENCES

ASTM (2012a) D 698-12e2: Standard test methods for laboratory compaction characteristics of soil using standard effort (12,400 ft-lbf/ft^3 (600 kN-m/m^3)). ASTM International, West Conshohocken, PA, USA.

ASTM (2012b) D 1557-12e1: Standard test methods for laboratory compaction characteristics of soil using modified effort (56,000 ft-lbf/ft^3 (2,700 kN-m/m^3)). ASTM International, West Conshohocken, PA, USA.

Avalle DL, Jaksa MB and Scott BT (2009) Ground energy and impact of rolling dynamic compaction – results from research test site. In *Proceedings of the 17th International Conference on Soil Mechanics and Geotechnical Engineering* (Hamza M, Shahien M and El-Mossallamy Y (eds)). IOS Press, Amsterdam, the Netherlands. pp. 2228–2231, https://doi.org/10.3233/978-1-60750-031-5-2228.

Bastaee B and Parvizi M (2012) Experimental and numerical analysis of impact roller on clay overlying sand. *Proceedings of the 15th International Conference on Experimental Mechanics, Porto, Portugal*, paper 2627.

Bradley AB, Crisp AC, Jiang JH and Power CN (2012) *Assessing the Effectiveness of Rolling Dynamic Compaction Using LS-DYNA*. School of Civil Environmental and Mining Engineering, University of Adelaide, Adelaide, Australia, Honours Research Report.

Brown D (2016) *Tracker Video Analysis and Modeling Tool*. See http://physlets.org/tracker/ (accessed 20/02/2018).

Clifford JM and Bowes G (1995) Calculating the energy delivered by an impact roller. *A Trilogy of Papers for the Sept. 1995 Lecture Tour and International Seminars to Commemorate the 10th Anniversary of the BH-1300 Impact Roller*, Paper 2, pp. 1–15.

Kim K (2010) *Impact Rollers (Soil Compaction) Numerical Simulation of Impact Rollers for Estimating the Influence Depth of Soil Compaction*, 1st edn. Lap Lambert Academic Publishing, Saarbrucken, Germany.

Kuo YL, Jaksa MB, Scott BT *et al.* (2013) Assessing the effectiveness of rolling dynamic compaction. *Proceedings of the 18th International Conference on Soil Mechanics and Geotechnical Engineering, Paris, France*, vol. 2, pp. 1309–1312.

SA (Standards Australia) (2003a) AS 1289.5.1.1: Soil compaction and density tests – determination of the dry density/moisture content relation of a soil using standard compactive effort. Standards Australia, Sydney, Australia.

SA (2003b) AS 1289.5.2.1: Soil compaction and density tests – determination of the dry density/moisture content relation of a soil using modified compactive effort. Standards Australia, Sydney, Australia.

Scott BT, Jaksa MB and Kuo YL (2012) Use of Proctor compaction testing for deep fill construction using impact rollers. In *Proceedings of International Conference of Ground Improvement & Ground Control, Wollongong, Australia*. Research Publishing Services, Wollongong, Australia, pp. 1107–1112, https://doi.org/10.3850/978-981-07-3560-9_04-0412.